




# Influence of P content on SMPs in Fe–Si–B–P–C–Cu–Nb amorphous alloys under longitudinal field annealing

Xuhang Zhang<sup>1,2</sup>, Yaqiang Dong<sup>1,3,\*</sup> , Changjiu Wang<sup>1</sup>, Aina He<sup>1,3,\*</sup>, Jiawei Li<sup>1,3</sup>, Fushan Li<sup>2,\*</sup>, Liang Chang<sup>1</sup>, Qiang Chi<sup>1</sup>, and Xiaoxue Shui<sup>4</sup>

<sup>1</sup>Zhejiang Province Key Laboratory of Magnetic Materials and Application Technology, CAS Key Laboratory of Magnetic Materials and Devices, Ningbo Institute of Materials Technology & Engineering, Chinese Academy of Sciences, Ningbo 315201, Zhejiang, China

<sup>2</sup>School of Materials Science and Engineering, Zhengzhou University, Zhengzhou 450001, Henan, China

<sup>3</sup>University of Chinese Academy of Sciences, Beijing 100049, China

<sup>4</sup>Analytical Center, Ningbo Institute of Materials Technology & Engineering, Chinese Academy of Sciences, Ningbo 315201, Zhejiang, China

Received: 26 November 2020

Accepted: 28 January 2021

Published online:

18 February 2021

© The Author(s), under exclusive licence to Springer Science+Business Media, LLC part of Springer Nature 2021

## ABSTRACT

The influence of P content on Curie temperature, magnetic properties and microstructures of  $\text{Fe}_{81.5}\text{Si}_3\text{B}_{10+x}\text{P}_{3.5-x}\text{C}_{0.2}\text{Cu}_{0.8}\text{Nb}_1$  ( $x = 0, 1, 2, \text{ and } 3$  at.%) alloys subjected to magnetic field annealing has been studied. Here, the decrease in P content can improve Curie temperature of alloys from about 575 to 584 K, which increases the operating temperature of magnetic device. Via optimal field annealing technique, the amorphous alloy with  $x = 3$  exhibits good soft magnetic properties, including saturation magnetic flux density of 1.53 T, high effective permeability above 12,000, low coercivity below 3 A/m, and low core loss around 0.18 W/kg. The hysteresis loops show that tuning down the content of P relative to B can increase the saturation magnetic flux density of alloy system. Besides, the investigation about the microstructures of alloys annealed at optimal conditions indicates that longitudinal magnetic field annealing can improve the stability of amorphous phase, thereby ensuring the amorphous structure annealed at a higher annealing temperature compared with the general annealing for alloys.

## 1 Introduction

Fe-based amorphous alloys have attracted both scientific and technological attentions due to their excellent soft magnetic properties (SMPs) including high saturation magnetic flux density ( $B_s$ ) and

effective permeability ( $\mu_e$ ), as well as low coercivity ( $H_c$ ) and core loss ( $P_i$ ), applied widely in electrical and electronic devices including transformer and amplifier switch [1–3]. However, compared to Si-steel, their relatively low  $B_s$  is not conducive to the development of device miniaturization. It is

Address correspondence to E-mail: dongyq@nimte.ac.cn; hean@nimte.ac.cn; fsli@zzu.edu.cn

increasingly important to develop the amorphous alloys with excellent SMPs.

There are mainly two ways to improve SMPs of alloys as followings: (1) optimizing elements including the increasing the content of ferromagnetic elements and the adjusting the content of metalloids elements. But excessive Fe content usually leads to the reduction of amorphous forming ability (AFA), which is not conducive to the mass production of amorphous alloys [4]. The addition of metals elements including Co and Nb etc. increases the cost of production to some extent [5]. Therefore, the adjusting the content of metalloid elements is an effective choice to improve SMPs without increasing the cost and decreasing the AFA of alloys. With investigating the mixing enthalpy between metalloid elements and Fe [6, 7], it was found that the substitution of B for P can increase the stability of amorphous matrix, which has aroused wide concerns of researchers. (2) Optimized annealing technique. Actually, there are three main types including general annealing (GA) [8], magnetic field annealing (MA) and rapid annealing (RA) at present. Compared with GA, RA and MA have unique advantages in improving SMPs of as-casting amorphous alloys, which has attracted extensive attention of researchers. But considering the harsh requirement of RA [9], MA is more hopeful to industrial production. Moreover, the related researches found that MA can apparently improve SMPs of alloys due to the additional magnetic anisotropy induced by the magnetic field [10–12]. Specifically, longitudinal magnetic field annealing (LMA) not only can improve the initial permeability, but changes the rectangular ratio of hysteresis loop, and thus reduce  $P_i$  of alloys due to that the direction of magnetic field is along to the stripe [13–15], which arouses the interest of scientific researchers. Therefore, to meet the development of miniaturization in magnetic device, we expect to optimize the microstructures and magnetic properties of alloys through slightly adjusting the content of P and B under LMA, and to develop a kind of alloy with excellent SMPs.

In this work,  $\text{Fe}_{81.5}\text{Si}_3\text{B}_{10+x}\text{P}_{3.5-x}\text{C}_{0.2}\text{Cu}_{0.8}\text{Nb}_1$  ( $x = 0, 1, 2, \text{ and } 3 \text{ at.}\%$ ) alloys with different P contents via LMA were synthesized to reveal the effect of P content on their microstructure and SMPs, which contributes to developing the alloys with excellent SMPs, and thus promotes the development of

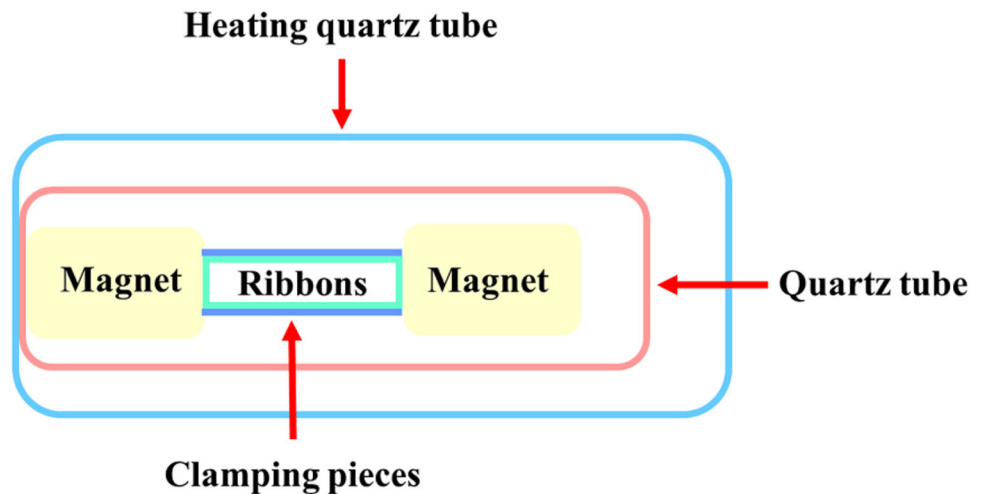
miniaturization and industrialization in magnetic device.

## 2 Experimental procedure

The alloy ingots with nominal composition of  $\text{Fe}_{81.5}\text{Si}_3\text{B}_{10+x}\text{P}_{3.5-x}\text{C}_{0.2}\text{Cu}_{0.8}\text{Nb}_1$  ( $x = 0, 1, 2, \text{ and } 3 \text{ at.}\%$ ) were prepared by induction melting high pure raw materials: Fe (99.97 wt%), Si (99.999 wt%), B (99.5 wt%), Cu (99.99 wt%), Nb (99.9 wt%), pre-alloyed Fe-P (15.6 wt%) and Fe-C (3.6 wt%) in a high purity argon atmosphere. The ribbons with a width of about 1 mm and a thickness of around 22  $\mu\text{m}$  were prepared via a single-roller melt-spinning technique, which was cut into a length of 50 mm for latter annealing and testing. Among the melt spinning experiment, the diameter of the quartz pipe orifice is about 0.75–0.8 mm, and the pressure difference between the inside and outside of quartz tube is 600 Pa.

The structures of ribbons were detected by X-ray diffraction (XRD, Bruker D8 Advance) with Cu  $K\alpha$  radiation. Curie temperature ( $T_c$ ) was analyzed via thermal gravity (TG/DTA, PerkinElmer Diamond) and magnetic property measurement system (MPMS, SQUID-VSM) at a heating rate of 10 K/min in a high purity argon, respectively. In TG experiments, to directly show the changes of weight, a magnetic field was applied in order to directly show the changes of weight. The isothermal annealing under LMA was carried out in a vacuum furnace and subsequently air cooling. The magnetic field intensity is 20 Oe that was controlled by a pair of AlNiCo permanent magnets which has high  $T_c$  in the quartz tube, and its schematic diagram is shown in Fig. 1. The magnetic properties of annealed ribbons including  $B_s$ ,  $H_c$ ,  $\mu_e$ , and  $P_i$  were measured with a vibrating sample magnetometer (VSM, Lake Shore 7410) under a field of 800 kA/m, a  $B$ - $H$  loop tracer (EXPH-100) under a field of 800 A/m, an impedance analyzer (Agilent 4294 A) under an applied magnetic field of 1 A/m at 1 kHz, and an AC  $B$ - $H$  loop tracer at 50 Hz under 1 T, respectively. Besides, when VSM measurements are made, the orientation of the strips with respect to the applied magnetic field is random with the aim of reducing anisotropy. For this purpose the strips were glued into the Chinese character “rice” shape on the sample cup. The microstructures of ribbons were characterized by transmission electron microscopy

**Fig. 1** The schematic diagram of LMA technique



(TEM, Talos F200x and TF20). The density of alloys was measured through the Archimedes method. All experimental data were measured repeatedly to ensure their repeatability and accuracy.

### 3 Results and discussion

#### 3.1 Characterizations of the melt-spun ribbons

The amorphous structures of  $\text{Fe}_{81.5}\text{Si}_3\text{B}_{10+x}\text{P}_{3.5-x}\text{C}_{0.2}\text{Cu}_{0.8}\text{Nb}_1$  ( $x = 0, 1, 2,$  and  $3$  at.%) alloys have been investigated by XRD in previous work [16]. The microstructures of ribbons were further detected via TEM as shown in Fig. 2. For all alloys, only a disordered and homogeneous structure is observed in the bright-field TEM images of Fig. 2a–d, and the corresponding selected area electron diffraction (SAED) patterns in Fig. 2e–h consist of halo diffraction rings, which confirms the formation of complete amorphous structure.

$T_c$  is an important thermodynamic parameter at which the ferromagnetic phase transforms to the paramagnetic phase for the magnetic alloys. When annealing temperature ( $T_a$ ) above it, the magnetic properties of alloys is more susceptible to the magnetic field. To better understand the role of P content on  $T_c$  of the alloy system, TG and MPMS measurements of melt-spun ribbons were performed, respectively. Figure 3 reveals the effect of P content on  $T_c$  from the variation trend of weight and magnetization with temperature, respectively. Both

Fig. 3a and b show that  $T_c$  moves to a higher temperature with the decrease in P content, ranging from about 575 to 584 K.  $T_c$  of amorphous alloys is closely related to the composition and its determined atomic interaction. According to the Slater–Pauling curve, as P content decreases together with B content increasing, the magnetic exchange interaction between iron atoms will be enhanced, leading to the increment of  $T_c$  [17–19]. Therefore, the substitution of B for P can improve  $T_c$  of alloy system, which raises the operating temperature of magnetic device.

#### 3.2 Magnetic properties variation with P content under LMA

Magnetic properties of amorphous alloys are sensitive to the annealing technique. LMA favors to improve SMPs of alloys. Figure 4 shows the dependencies of (a)  $B_s$ , (b)  $H_c$ , (c)  $\mu_e$  and (d)  $P_i$  on  $T_a$  for the alloy system in LMA process. As depicted in Fig. 4a, there is only a slight fluctuation in  $B_s$  with  $T_a$  increasing, but  $B_s$  ranges from about 1.5 to 1.53 T with P content decreasing, which indicates that the decrease in P content is the main factor for improving  $B_s$ . The replacement of P by B with smaller atomic size shortens the distance between Fe atoms and thus enhances the magnetic exchange between Fe atoms, which accounts for the increase of  $B_s$  as P content reduces [20, 21]. Under LMA process, SMPs including  $H_c$ ,  $\mu_e$  and  $P_i$  of alloys are more susceptible to  $T_a$ . It is obvious that  $H_c$  rapidly decreases from above 12 to around 3 A/m under the combination of increasing  $T_a$  and decreasing P content in Fig. 4b.

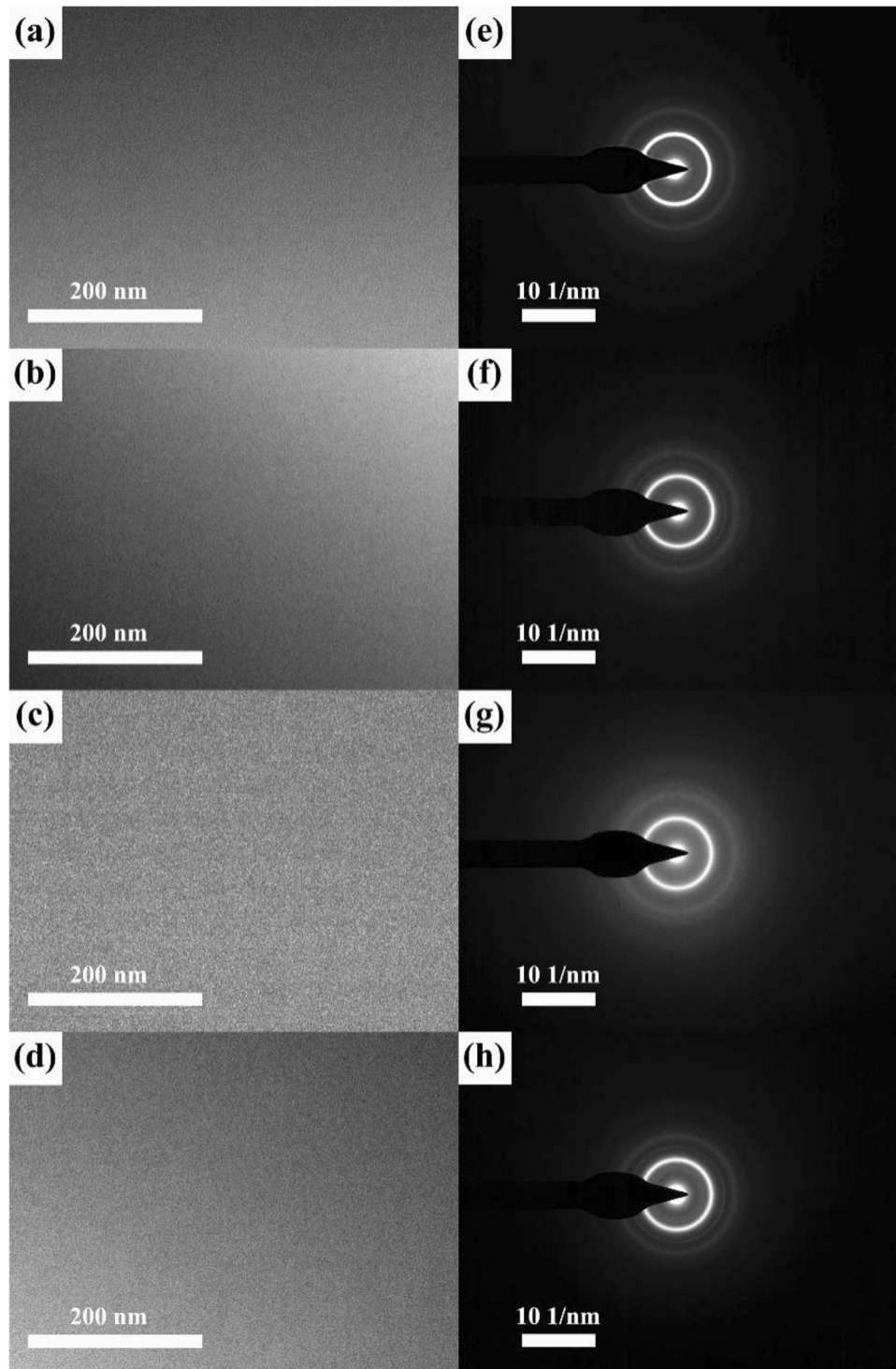


**Fig. 2** a–d Bright-field TEM images and e–h corresponding SAED of  $\text{Fe}_{81.5}\text{Si}_3\text{B}_{10+x}\text{P}_{3.5-x}\text{C}_{0.2}\text{Cu}_{0.8}\text{Nb}_1$  ( $x = 0, 1, 2,$  and  $3$  at.%) alloys

Meanwhile,  $\mu_e$  at 1 kHz of alloys exhibits a trend contrary to that of  $H_c$ , and ranges from about 3300 to above 12,000 with  $T_a$  increasing under considering the influence of P content in Fig. 4c. And  $x = 3$  ( $\text{Fe}_{81.5}\text{Si}_3\text{B}_{13}\text{P}_{0.5}\text{C}_{0.2}\text{Cu}_{0.8}\text{Nb}_1$ ) alloy exhibits higher  $\mu_e$ ,

which indicates that the substitution of B for P can increase  $\mu_e$  of alloys in LMA process. In Fig. 4d, subjected to the common influence of rising  $T_a$  and changing P content,  $P_{10/50}$  (measured at  $f = 50$  Hz under  $B_m = 1$  T) of alloys shows the similar trend to

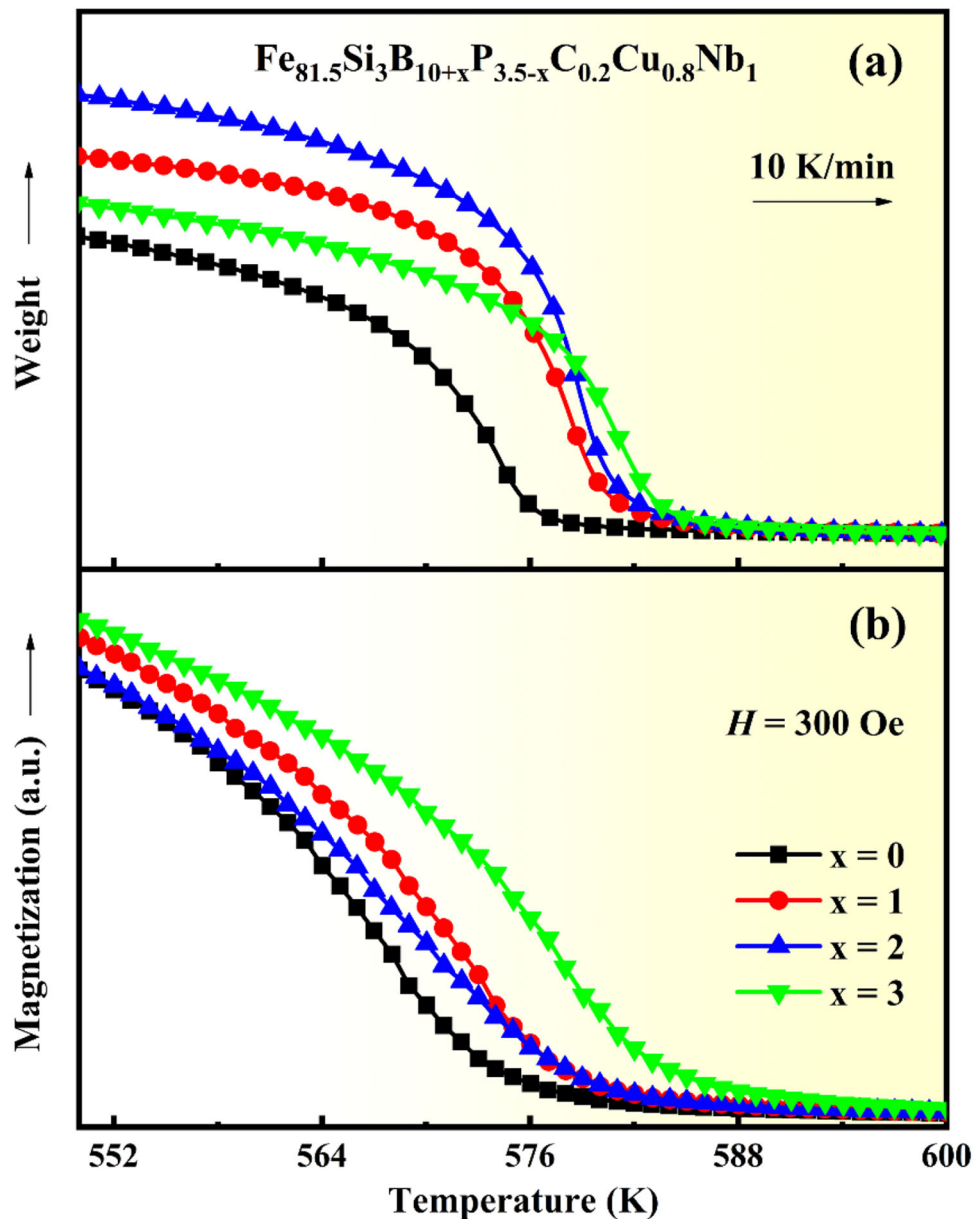


**Fig. 3** a TG and b  $M$ - $T$  curves of  $\text{Fe}_{81.5}\text{Si}_3\text{B}_{10+x}\text{P}_{3.5-x}\text{C}_{0.2}\text{Cu}_{0.8}\text{Nb}_1$  ( $x = 0, 1, 2,$  and  $3$  at.%) amorphous alloys

$H_c$ , which decreases from around 0.8 to 0.18 W/kg. And  $P_{10/50}$  of  $x = 3$  alloy exhibits the lowest values, which suggests that the decrease in P content can effectively reduce  $P_{10/50}$  of alloys in LMA process. From the results of Fig. 4, the optimal  $T_a$  for the excellent SMPs of alloy system is about 833 K. Among the alloy system,  $x = 3$  alloy exhibits the optimum performance including high  $B_s$  of 1.53 T, low  $H_c$  of 2.9 A/m, high  $\mu_e$  of above 12,000, and low  $P_{10/50}$  of 0.18 W/kg. Therefore, proper decrease in P content can boost SMPs of alloys, with an optimal 0.5 at.% P content for the alloy system in the LMA process. The

reason of this phenomenon may be due to that little outer electrons of P atoms dope with that of Fe atoms and thus some of them may fill up the  $3d$  bands of Fe atoms, which increases the magnetic moment of Fe atoms and causes the enhancement of exchange interactions, and thus improves SMPs of alloys with the substitution of B for P content [22, 23].

LMA technique can effectively improve  $\mu_e$  of alloys. In order to evaluate the influence of LMA on  $\mu_e$  for  $x = 3$  alloy, the frequency spectrum of  $\mu_e$  annealed at different  $T_a$  were tested. Figure 5 reveals the changes in  $\mu_e$  with frequency at different  $T_a$  of

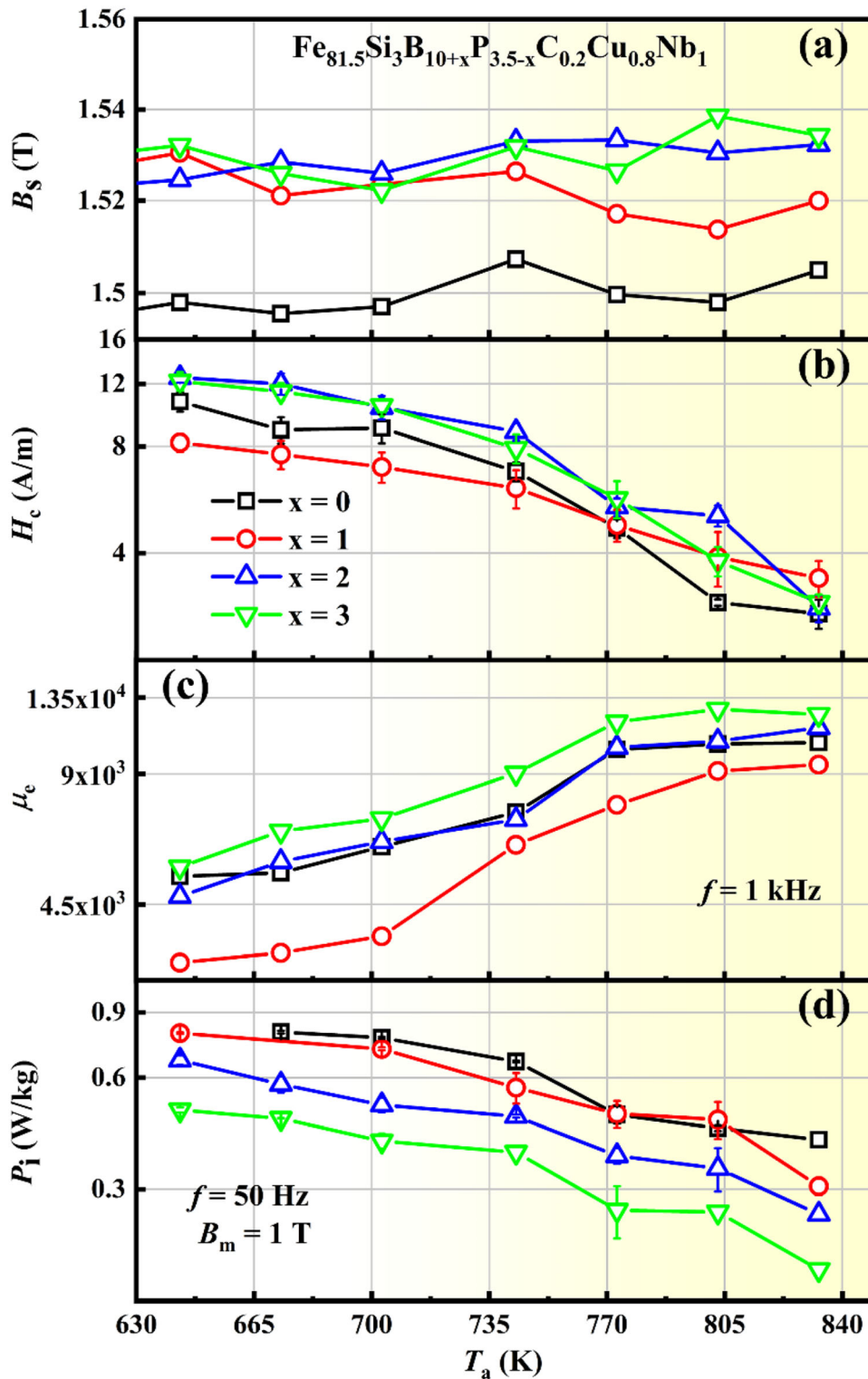


**Fig. 4** The dependencies of **a**  $B_s$ , **b**  $H_c$ , **c**  $\mu_e$ , and **d**  $P_i$  on  $T_a$  of  $Fe_{81.5}Si_3B_{10+x}P_{3.5-x}C_{0.2}Cu_{0.8}Nb_1$  ( $x = 0, 1, 2$ , and  $3$  at.%) amorphous alloys in LMA process

$x = 3$  alloy in LMA process. As shown in Fig. 5,  $\mu_e$  of  $x = 3$  alloy approximately doubles when annealed at  $T_a$  ranging below 800 K (from 643 to 773 K) in a wide

frequency range (from 1 to 25 kHz). When annealed at  $T_a$  higher than 800 K, such as 803 and 833 K,  $\mu_e$  greatly attenuates with frequency increasing,

**Fig. 5** The trend of  $\mu_e$  with frequency at different  $T_a$  of  $x = 3$  alloy in LMA process

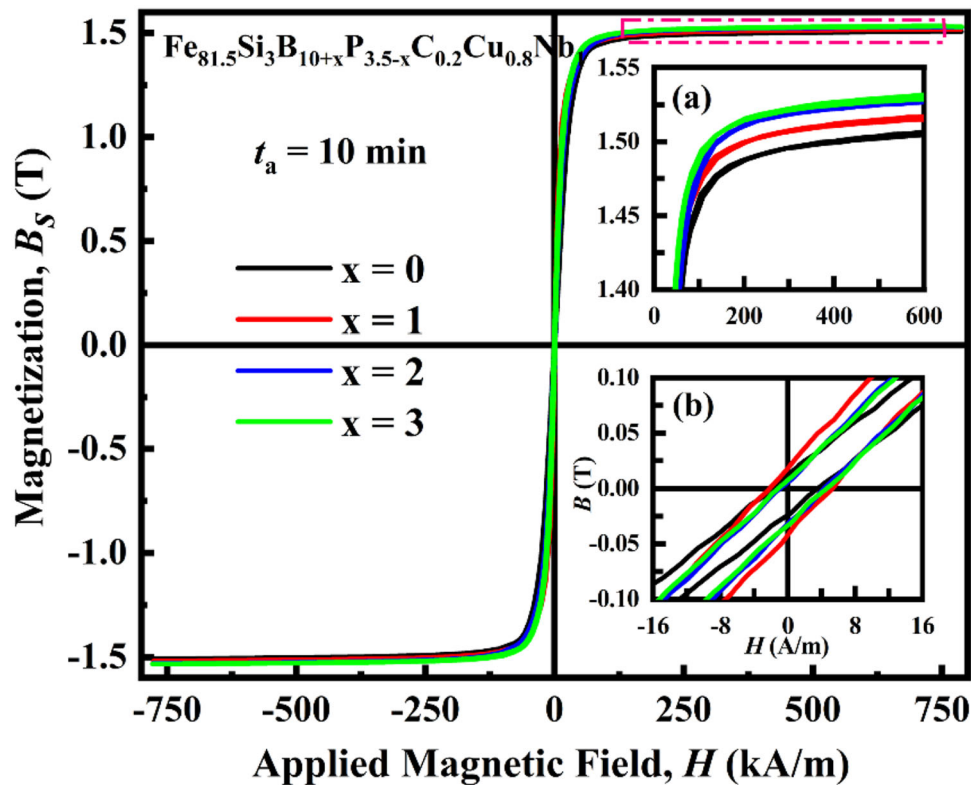
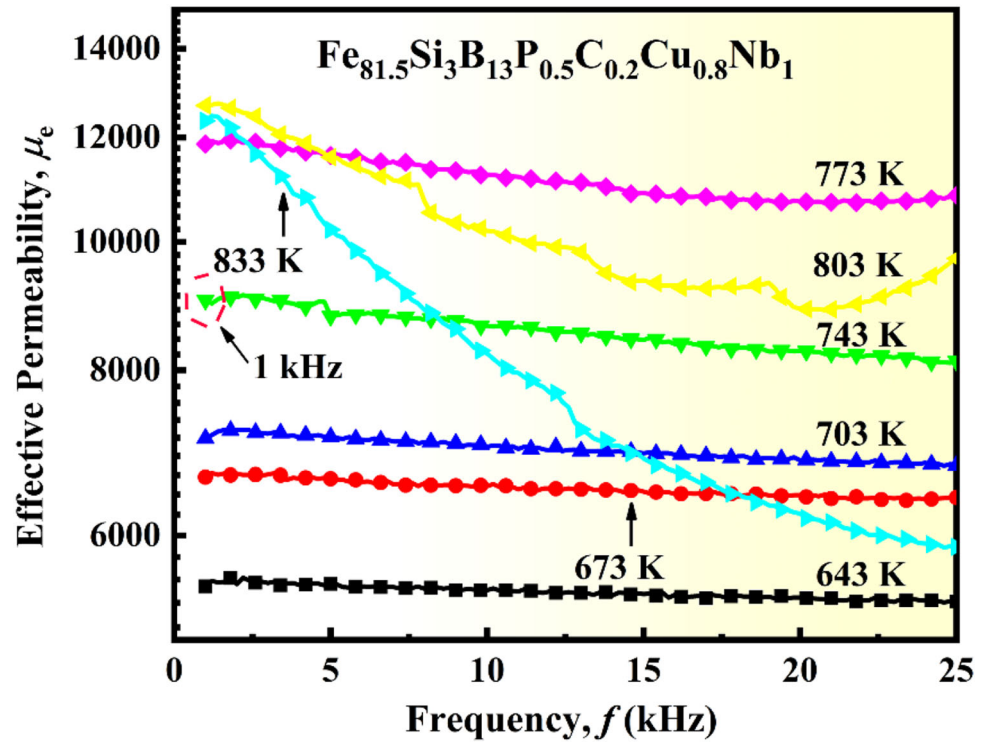


**Fig. 6** Hysteresis loops including inset (a) its partial enlarged graphs and inset (b) enlarged  $B$ – $H$  loops of  $\text{Fe}_{81.5}\text{Si}_3\text{B}_{10+x}\text{P}_{3.5-x}\text{C}_{0.2}\text{Cu}_{0.8}\text{Nb}_1$  ( $x = 0, 1, 2,$  and  $3$  at.%) amorphous alloys annealed at optimal conditions

although it is still improved greatly at 1 kHz. Resultantly, LMA can advance  $\mu_e$  of  $x = 3$  alloy to above 12,000 at low frequency.

Figure 6 is the hysteresis loops of alloy system annealed at optimal conditions. All curves present the typical characteristics of soft magnetic alloys, and  $B_s$  ranges from about 1.50 to 1.53 T as P content decreases from 3.5 to 0.5 at.%, which shows that the reduction of P content contributes to the rising of  $B_s$ . Besides, inset (b) demonstrates that  $H_c$  of  $x = 3$  alloy closes to that of the initial alloy, implying that the decrease in P content can enhance  $B_s$  without deteriorating SMPs of alloys.

### 3.3 Microstructure variation with P content under LMA

To further understand the magnetic properties changes of alloys annealed at optimal conditions in LMA process, the relevant microstructures were detected via XRD and TEM, respectively. As described in Fig. 7, all curves exhibit typical diffuse scattering peaks without apparent crystallization peak, except that the diffraction peak of  $x = 0$  ( $\text{Fe}_{81.5}\text{Si}_3\text{B}_{10}\text{P}_{3.5}\text{C}_{0.2}\text{Cu}_{0.8}\text{Nb}_1$ ) alloy is slightly tapered. The

Fig. 8 a–d bright-field TEM images and e–h corresponding SAED of  $\text{Fe}_{81.5}\text{Si}_3\text{B}_{10+x}\text{P}_{3.5-x}\text{C}_{0.2}\text{Cu}_{0.8}\text{Nb}_1$  ( $x = 0, 1, 2,$  and  $3$  at.%) alloys annealed at optimal conditions

microstructures were further examined by TEM. Except that some  $\alpha$ -Fe clusters appear in  $x = 0$  alloy as shown in the bright-field TEM images of Fig. 8a, only a disordered and homogeneous structure is seen in that of Fig. 8b–d with the corresponding SAED patterns in Fig. 8f–h consisting of halo diffraction rings. These identification results indicate that an amorphous phase is maintained in all alloys except  $x = 0$  alloy annealed at optimal conditions. Therefore, stress release events mainly occur in LMA process, which not only decreases the free volume and defects, but makes the amorphous structure more homogeneous and magnetic domains more ordered, and thus SMPs of alloys get improved [24, 25]. Besides, compared with the nanocrystal structures of GA annealed at 833 K in previous work [16], it was found that the alloys exhibit apparent amorphous structure of LMA annealed at 833 K, which indicates that LMA technique can improve the stability of

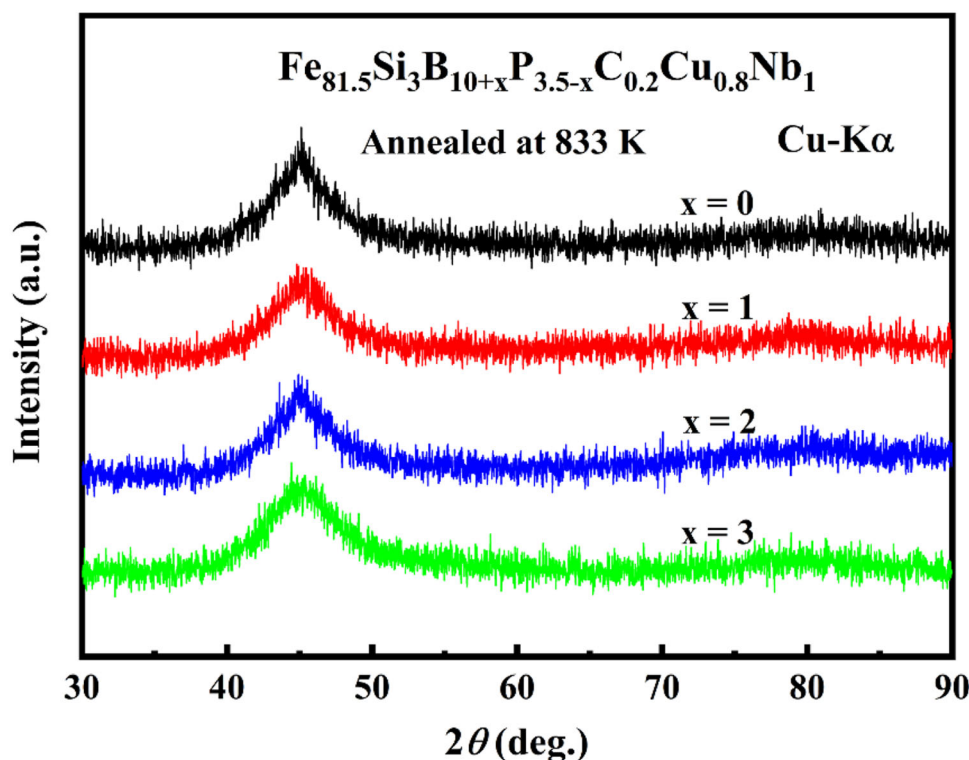
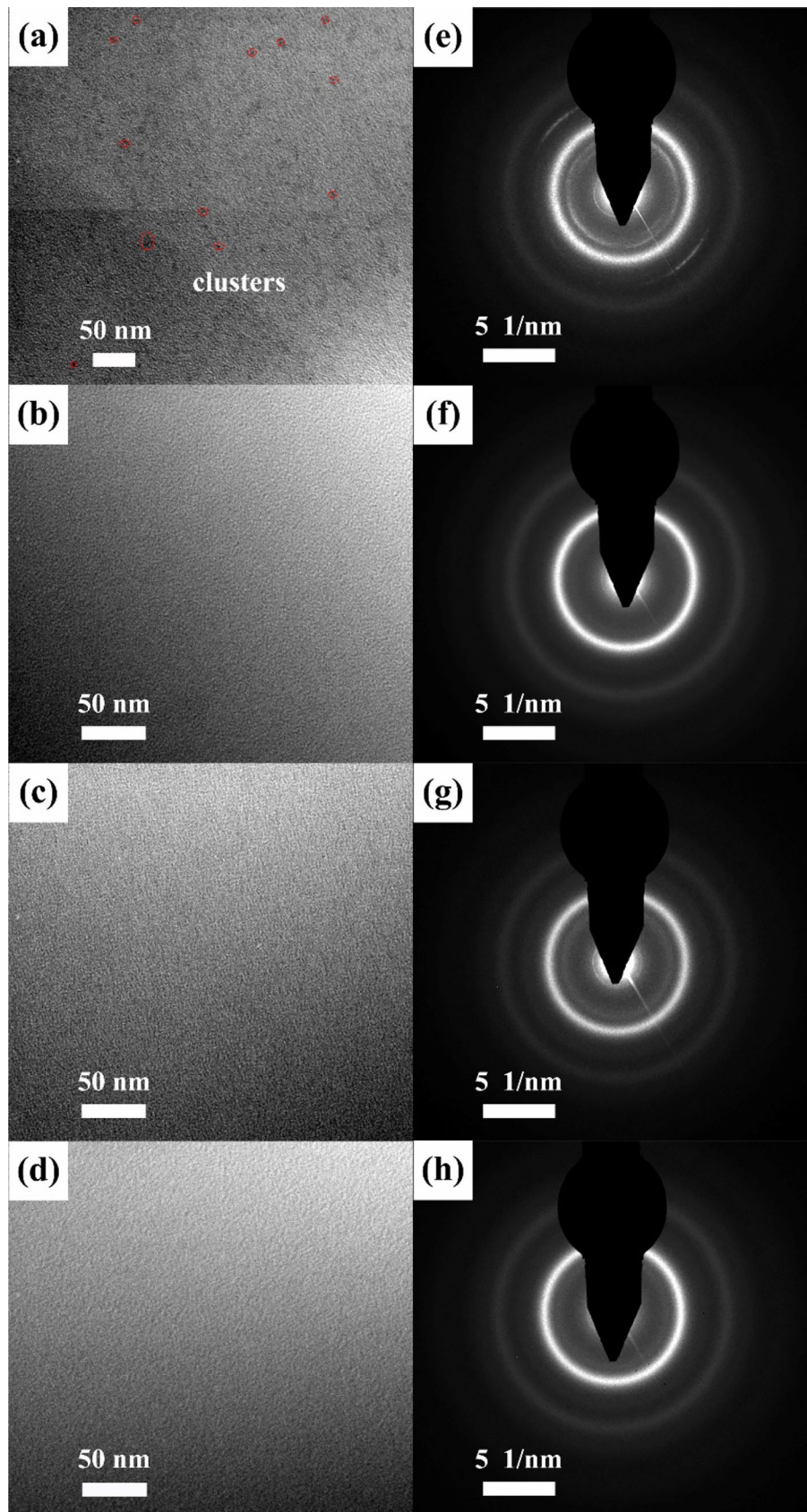


Fig. 7 XRD patterns of  $\text{Fe}_{81.5}\text{Si}_3\text{B}_{10+x}\text{P}_{3.5-x}\text{C}_{0.2}\text{Cu}_{0.8}\text{Nb}_1$  ( $x = 0, 1, 2,$  and  $3$  at.%) alloys annealed at optimal conditions





**Table 1**  $B_s$  and  $H_c$  of  $x = 3$  alloy compared with the other alloys

Alloys	$B_s$ (T)	$M_s$ (emu/g)	$H_c$ (A/m)
$x = 3$ (the present work)	1.53	161.1	2.9
$\text{Fe}_{84}\text{B}_8\text{P}_{3.5}\text{Mo}_2\text{Cu}_1$ [26]	1.39	–	4.4
$\text{Fe}_{84}\text{B}_8\text{P}_4\text{Mo}_2\text{Si}_2$ [27]	1.53	–	7.3
$\text{Fe}_{77}\text{B}_{9.5}\text{P}_{10.5}\text{Nb}_2\text{Cr}_1$ [28]	1.30	–	3.8
$\text{Fe}_{83.3}\text{Si}_2\text{B}_{14}\text{Cu}_{0.5}\text{C}_{0.2}$ [29]	–	151.5	4.0

amorphous phase and thus ensure the amorphous structure even annealed at a higher  $T_a$ .

Table 1 lists  $B_s$  and  $H_c$  of  $x = 3$  alloy compared with  $\text{Fe}_{84}\text{B}_8\text{P}_{3.5}\text{Mo}_2\text{Cu}_1$  [26],  $\text{Fe}_{84}\text{B}_8\text{P}_4\text{Mo}_2\text{Si}_2$  [27],  $\text{Fe}_{77}\text{B}_{9.5}\text{P}_{10.5}\text{Nb}_2\text{Cr}_1$  [28], and  $\text{Fe}_{83.3}\text{Si}_2\text{B}_{14}\text{Cu}_{0.5}\text{C}_{0.2}$  [29] alloys. Although  $\text{Fe}_{84}\text{B}_8\text{P}_4\text{Mo}_2\text{Si}_2$  alloy has similar  $B_s$  with the present alloy, it has higher  $H_c$ . Compared with the other alloys, the present alloy exhibits better SMPs including high  $B_s$  of about 1.53 T ( $M_s \approx 161$  emu/g) and low  $H_c$  of 2.9 A/m via LMA, which promises the industrialization and miniaturization of magnetic device

## 4 Conclusions

In conclusion, the influence of P content on  $T_c$ , microstructures, and SMPs of Fe–Si–B–P–C–Cu–Nb amorphous alloys via LMA were investigated in detail. The obtained results can be summarized as follows:

1. The optimized amorphous microstructures could significantly improve SMPs via slightly adjusting P content and LMA for the present alloy system. As a result,  $x = 3$  alloy exhibits good SMPs, including high  $B_s$  of 1.53 T, low  $H_c$  of 2.9 A/m, high  $\mu_e$  of above 12,000, and low  $P_{10/50}$  of around 0.18 W/kg.
2. The substitution of B for P can improve  $T_c$  of alloy system from about 575 to 584 K, which increases the operating temperature of magnetic device.
3. The combination of LMA and tuning down the content of P can double  $\mu_e$  at 1 kHz of  $x = 3$  alloy, exceeding 12,000.
4. Compared with GA, LMA can improve the stability of amorphous phase and thus ensure the amorphous structure even annealed at a higher  $T_a$  for the present alloys.

## Author contributions

Xuhang Zhang, Yaqiang Dong and Fushan Li contributed the central idea, and wrote the first draft. Aina He and Jiawei Li contributed to improve the manuscript. Liang Chang contributed to provide the component ideas. Changjiu Wang, Qiang Chi and Xiaoxue Shui completed the remain refining experiment. All authors have contributed to the manuscript.

## Funding

This work was supported by the National Natural Science Foundation of China (grant number U1704159), the National Natural Science Foundation of China (Grant No.51771083), and the S&T Innovation 2025 Major Special Program (Grant Number 2018B10084).

## Compliance with ethical standards

**Conflict of interest** The authors declare that they have no known competing financial interests or personal relationships that could have appeared to influence the work reported in this paper.

## References

1. J. Xu, Y.Z. Yang, Q.S. Yan, C.F. Fan, F.T. Hou, Z.W. Xie, Effect of microalloying on crystallization behavior, magnetic properties and bending ductility of high Fe content FeSiB–CuPC alloys. *J. Alloy Compd.* **777**, 499–505 (2019)
2. F. Wang, A. Inoue, Y. Han, S.L. Zhu, F.L. Kong, E. Zanaeva, G.D. Liu, E. Shalaan, F. Al-Marzouki, A. Obaid, Excellent soft magnetic Fe–Co–B-based amorphous alloys with extremely high saturation magnetization above 1.85 T and low coercivity below 3 A/m. *J. Alloy Compd.* **711**, 132–142 (2017)
3. A. Urata, H. Matsumoto, S. Sato, A. Makino, High  $B_s$  nanocrystalline alloys with high amorphous-forming ability. *J. Appl. Phys.* **105**, 07A324-1-07A324-3 (2009)
4. H.R. Lashgari, D. Chu, S.S. Xie, H.D. Sun, M. Ferry, S. Li, Composition dependence of the microstructure and soft magnetic properties of Fe-based amorphous/nanocrystalline alloys: a review study. *J. Non-Cryst. Solids* **391**, 61–82 (2014)
5. F. Wang, A. Inoue, Y. Han, F.L. Kong, S.L. Zhu, E. Shalaan, F. Al-Marzouki, A. Obaid, Soft magnetic Fe–Co-based

- amorphous alloys with extremely high saturation magnetization exceeding 1.9 T and low coercivity of 2 A/m. *J. Alloy Compd.* **723**, 376–384 (2017)
6. A. Takeuchi, A. Inoue, Mixing enthalpy of liquid phase calculated by miedema's scheme and approximated with sub-regular solution model for assessing forming ability of amorphous and glassy alloys. *Intermetallics* **18**, 1779–1789 (2010)
  7. A. Takeuchi, A. Inoue, Classification of bulk metallic glasses by atomic size difference, heat of mixing and period of constituent elements and its application to characterization of the main alloying element. *Mater. Trans.* **12**, 2817–2829 (2005)
  8. B. Majumdar, D. Akhtar, Structure and coercivity of nanocrystalline Fe–Si–B–Nb–Cu alloys. *Bull. Mater. Sci.* **28**, 395–399 (2005)
  9. K.G. Pradeep, G. Herzer, P. Choi, D. Raabe, Atom probe tomography study of ultrahigh nanocrystallization rates in FeSiNbBCu soft magnetic amorphous alloys on rapid annealing. *Acta Mater.* **68**, 295–309 (2014)
  10. B.S. Berry, W.C. Pritchett, Magnetic annealing and directional ordering of an amorphous ferromagnetic alloy. *Phys. Rev. Lett.* **34**, 1022–1025 (1975)
  11. S. Kwon, S. Kim, H. Yim, Improvement of saturation magnetic flux density in Fe–Si–B–Nb–Cu nanocomposite alloys by magnetic field annealing. *Curr. Appl. Phys.* **20**, 37–42 (2020)
  12. Y. Yoshizawa, K. Yamauchi, Effects of magnetic field annealing on magnetic properties in ultrafine crystalline Fe–Cu–Nb–Si–B alloys. *IEEE Trans. Magn.* **25**, 3324–3326 (1989)
  13. H. Li, A.N. He, A.D. Wang, L. Xie, Q. Li, C.L. Zhao, G.Y. Zhang, P.B. Chen, Improvement of soft magnetic properties for distinctly high Fe content amorphous alloys via longitudinal magnetic field annealing. *J. Magn. Magn. Mater.* **471**, 110–115 (2019)
  14. I. Škorvánek, J. Marcin, J. Turčanová, J. Kováč, P. Švec, Improvement of soft magnetic properties in Fe<sub>38</sub>Co<sub>38</sub>Mo<sub>8</sub>B<sub>15</sub>Cu<sub>1</sub> amorphous and nanocrystalline alloys by heat treatment in external magnetic field. *J. Alloy. Compd.* **504**, S135–S138 (2010)
  15. M. Ghanaatshoar, N. Nabipour, M.M. Tehranchi, S.M. Hamidi, S.M. Mohseni, The influence of laser annealing in the presence of longitudinal weak magnetic field on asymmetrical magnetoimpedance response of CoFeSiB amorphous ribbons. *J. Non-Cryst. Solids* **354**, 5150–5152 (2008)
  16. X.H. Zhang, Y.Q. Dong, A.N. He, L. Xie, F.S. Li, L. Chang, H.Y. Xiao, H. Li, T. Wang, Improvement of SMPs in Fe–Si–B–P–C–Cu–Nb alloys via harmonizing P and B. *J. Magn. Magn. Mater.* **506**, 199757 (2020)
  17. Y.S. Tyan, L.E. Toth, Slater pauling magnetization curve in transition metal phosphides. *J. Electron. Mater.* **3**, 1–6 (1974)
  18. Y. Kakehashi, O. Hosohata, Curie-temperature “Slater-Pauling Curve”. *J. Phys. Colloque* **49**, C8–C73 (1988)
  19. C. Takahashi, M. Ogura, H. Akai, First-principles calculation of the Curie temperature Slater-Pauling curve. *J. Phys.-Condens. Matter.* **19**, 365233 (2007)
  20. M.Q. Zuo, S.Y. Meng, Q. Li, H.X. Li, C.T. Chang, Y.F. Sun, Effect of metalloid elements on magnetic properties of Fe-based bulk metallic glasses. *Intermetallics* **83**, 83–86 (2017)
  21. S.Y. Meng, H.B. Ling, Q. Li, J.J. Zhang, Development of Fe-based bulk metallic glasses with high saturation magnetization. *Scripta Mater.* **81**, 24–27 (2014)
  22. Z.Q. Liu, M.J. Shi, T. Zhang, Composition dependences and optimization of the magnetic properties of Fe-based metallic glasses. *Mater. Res. Express* **1**, 046110 (2014)
  23. R.C. O’Handley, D.S. Boudreaux, Magnetic properties of transition metal-metalloid glasses a charge transfer model. *Phys. Status Solidi (a)* **45**, 607–615 (1978)
  24. H. Kronmüller, M. Fähnle, M. Domann, H. Grimm, R. Grimm, B. Gröger, Magnetic properties of amorphous ferromagnetic alloys. *J. Magn. Magn. Mater.* **13**, 53–70 (1979)
  25. H.Y. Xiao, A.D. Wang, J.W. Li, A.N. He, T. Liu, Y.Q. Dong, H. Guo, X.C. Liu, Structural evolutionary process and interrelation for FeSiBNbCuMo nanocrystalline alloy. *J. Alloy Compd.* **821**, 153487 (2020)
  26. E.N. Zanaeva, A.I. Bazlov, D.A. Milkova, A.Y. Churyumov, A. Inoue, N.Y. Tabachkova, F. Wang, F.L. Kong, S.L. Zhu, High-frequency soft magnetic properties of Fe–Si–B–P–Mo–Cu amorphous and nanocrystalline alloys. *J. Non-Cryst. Solids* **526**, 119702 (2019)
  27. Y. Han, F.L. Kong, F.F. Han, A. Inoue, S.L. Zhu, E. Shalaan, F. Al-Marzouki, New Fe-based soft magnetic amorphous alloys with high saturation magnetization and good corrosion resistance for dust core application. *Intermetallics* **76**, 18–25 (2016)
  28. H. Matsumoto, A. Urata, Y. Yamada, A. Inoue, Novel FePBNbCr glassy alloys “SENNTIX” with good soft-magnetic properties for high efficiency commercial inductor cores. *J. Alloy Compd.* **509**, S193–S196 (2011)
  29. J. Xu, Y.Z. Yang, W. Li, X.C. Chen, The effect of introduction of carbon on the glass forming ability and magnetic properties of melt-spun Fe–Si–B–Cu–C alloys. *J. Non-Cryst. Solids* **447**, 167–170 (2016)

**Publisher’s note** Springer Nature remains neutral with regard to jurisdictional claims in published maps and institutional affiliations.